Facile Synthesis of Perovskite-Type Sm₁₋ₓSrₓMnO₃ (0 ≤ x ≤ 0.8), a Non-Precious Metal Oxides and its Electrocatalytic Analysis towards the Oxygen Evolution Reaction (OER)

Prakhar Mishra, Priya Sharma, Narendra Kumar Singh[*]

Department of Chemistry, Faculty of Science, University of Lucknow, Lucknow, India
Corresponding Author Email: nksbhu@yahoo.com; singh_narendra@lkouniv.ac.in Mobile: +91-9451949105

ABSTRACT

LaNiO₃, La₁₋ₓSrₓCoO₃, La₁₋ₓSrₓMnO₃ are a few examples of the perovskite-type oxides that hold great potential to be used as catalysts in numerous technologically significant processes such as the electrocatalysis of the oxygen evolution reaction [1-4], CO and hydrocarbons oxidation and the nitrogen oxides reduction [5]. Keeping this in mind, the present study brings up the synthesis of Strontium based Samarium Perovskite manganites (Sm1-xSrxMnO3 (0 ≤ x ≤ 0.8)) by a sol-gel low-temperature technique using malic acid. The physicochemical characterization of the synthesized electrocatalyst is done by using Scanning Electron Microscopy (SEM) and X-ray diffraction (XRD) technique. Furthermore, the electrocatalytic analysis towards water electrolysis were done by performing cyclic voltammetry between 0 and 0.7 V & Tafel experiments. Apart from this the perovskites have been also analysed for their kinetic and thermodynamic parameters. Among the prepared oxide catalysts, Sm₀.₆Sr₀.₄MnO₃ was found to be most electrocatalytically active with a current density of 126.6mA/cm² at 800mV and a Tafel slope of 112 mV decade⁻¹.

1. INTRODUCTION

Fossil fuels are becoming harder to come by, and people are becoming more aware of the environmental and geopolitical issues that come with their use, which has spurred significant work on the generation of innovative energy storage and conversion systems using materials that are affordable, abundant, and environmentally safe. Higher power and more energy-efficient storage devices, such as low-temperature fuel cells and rechargeable metal-air batteries that runs on electrocatalysis, have become the centre of attraction in the field of renewable energy. Both, the oxygen reduction $(O_2 + 4H^+ + 4e^- \rightarrow 2H_2O$; oxygen reduction reaction; ORR) and the water electrolysis $(2H_2O \rightarrow O_2 + 4H^+ + 4e^-$; oxygen evolution reaction; OER) are the fundamental techniques for generating green energy, but because of their sluggish kinetics, they require an appropriate electrocatalyst. Another challenge is that the efficient electrocatalysts for water splitting are economically unfavoured and comprised of rare noble metals, so not only the cost friendly but also more lucrative approaches are required for the encountering the efficient electrocatalysts based on earth abundant elements only.

The previous reports [6] also describes a technique for differential design of metal oxide as a electrocatalysts for the OER. It came up with the catalysts which was non-noble metals-based perovskite structure and that have a much better efficiency than the states of-the-art catalysts, iridium oxide. Furthermore, S. K. Tiwari et al. [7] synthesized Sr-substituted lanthanum cobaltates and reported that it has much more electrocatalytic efficiency than those previously prepared by conventional ceramic or thermal decomposition methods [8-12]. In addition to this they also reported the high electrochemically active surface area of the oxide (specially of La₀.₂Sr₀.₈CoO₃) with the same oxide obtained by nitrate decomposition [7]. These results promoted us to test the electrocatalytic activity of such type of perovskite oxides prepared by a low-temperature sol-gel route.

This paper focuses the synthesis and physicochemical characterization of Perovskite Oxide (Sm₁₋ₓSrₓMnO₃) using malic acid sol get route as an active electrocatalyst for water electrolysis.

2. EXPERIMENTAL

Perovskite-type oxides Sm₁₋ₓSrₓMnO₃ (0 ≤ x ≤ 0.8) were synthesised by low temperature sol gel route as reported by Teraoka et al. [13]. Stoichiometric amount of Sm(NO₃)₃.6H₂O (Merck 99.9%), Sr(NO₃)₂ (Merck 39.5-43.5%), Mn(CH₃COO)₂.4H₂O (Merck 99.5%) and the malic acid in excess amount were dissolved in 500 ml distilled water. The ammonia solution was added dropwise in above solution in order to maintain the pH. The mixture so obtained was heated over a water bath at 70°C until a gel like mass was obtained which was further decomposed and crushed into fine powder in agate pastel mortar. The powder so obtained was purified by sintering at 650°C for 5h to get the desired oxide material.

The crystal structure of the synthesized oxide was determined by using X-ray diffractometer provided with radiation source Cu-Kα (λ = 1.54056 Å). The Scanning Electron Microscope (SEM) was used to determine the morphology of the oxide powder.

The Perovskite oxides were studied for their oxygen evolution behaviour in alkaline medium in the form of film electrode prepared by oxide slurry painting technique on Ni-

support [14]. The potentiostat/galvanostat electrochemical system consisting of corrosion and electrochemical analytical software (Gamry Reference 600 ZRA) was used to perform Cyclic Voltammetry (CV) and Tafel experiments in a single compartment three-electrode glass cell. The oxide film electrode, Hg/HgO /1M KOH and Pt-foil were used as working, reference and auxiliary electrodes respectively. The electrical contact between the reference electrode and the electrolyte was made via a Luggin capillary (KCl/Agar-Agar salt bridge) to minimize the solution resistance (iR drop).

3. RESULT AND DISCUSSION

3.1 Physicochemical Characterization

3.1.1 Scanning Electron Micrograph (SEM)

Fig. 1 represents the SE-micrograph of pure and Sr-Substituted Samarium Manganite powder sintered at 650°C for 5hrs. Morphological structure of oxide powders appeared to be similar with each oxide. A crust like structure has been observed in the micrograph.

SmMnO₃ (pH=3.5)   Sm₀.₆Sr₀.₄MnO₃ (pH=3.5)

Sm₀.₂Sr₀.₈MnO₃ (pH=3.5)
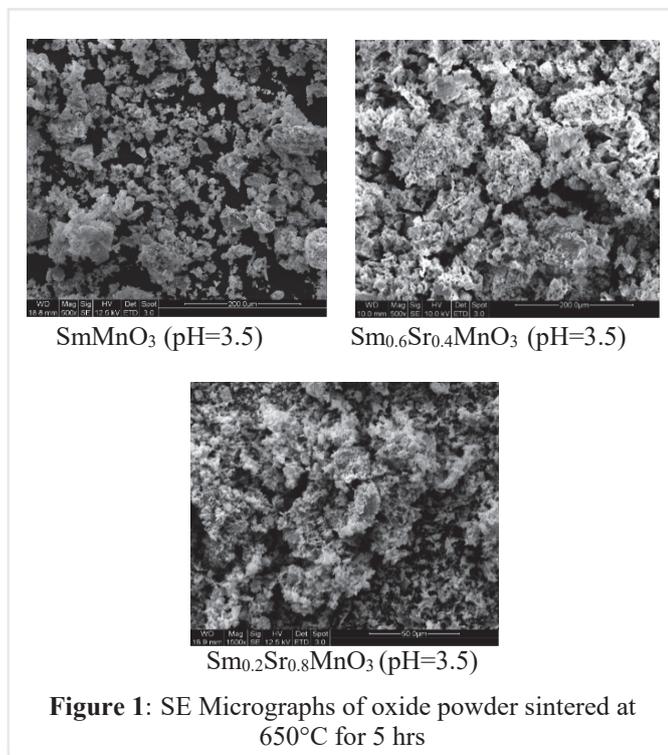
Figure 1: SE Micrographs of oxide powder sintered at 650°C for 5 hrs

3.1.2 X-ray diffraction

Crystal structure of Samarium Strontium Manganese oxides was investigated by X-ray diffraction (Fig. 2) by Panalytical X-pert 3 powder diffractometer with step size 0.013° and time per step 29s using Cu-K$_\alpha$=1.5405Å. The obtained XRD patterns are the same which are associated to those in COD ID 1006169. The results of powder XRD analysis of the materials showed that it has a Monoclinic crystal structure of space group P 21/a. The quality factors of the refinement are in acceptable range with χ^2 value 2.4352 for Sm₀.₆Sr₀.₄MnO₃. The x-ray diffraction patterns of the samples were refined using Rietveld method to calculate accurate unit cell dimensions as given in Table 1. The Scherer's formula [15],

$$D = \frac{0.9\,\lambda}{\beta Cos\,\theta}$$

was used to calculate the crystallite size of the material, where λ is the wavelength of Cu-Kα radiation source, β is the full width at half maximum of peak (FWHM) and θ is the diffraction angle and values are given in Table 1. The refined plot and the crystal structure obtained by using vesta software is shown in fig. 3.
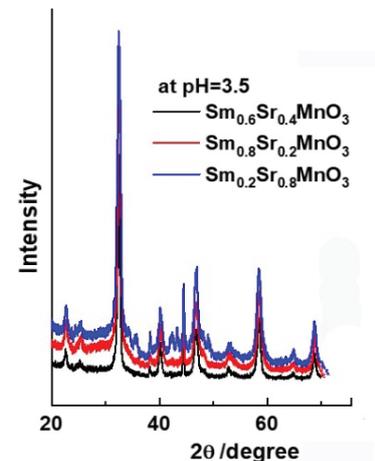
Figure 2: XRD powder patterns Sintered at 650°C for 5h
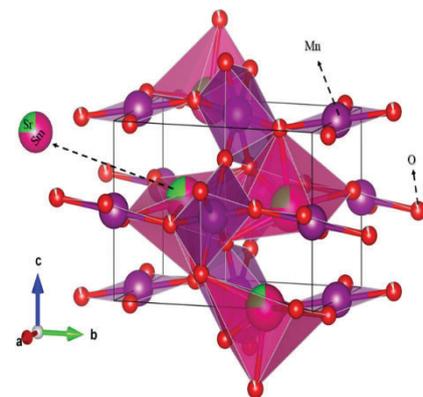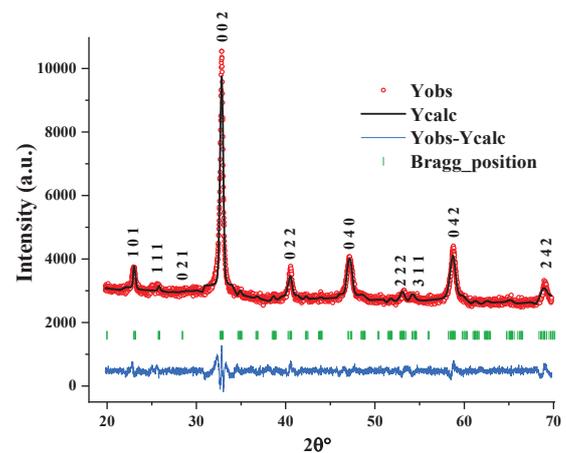
Figure 3 The profile plot and the crystal structure of Sm₀.₆Sr₀.₄MnO₃

Table 1 Lattice parameters for oxide powder sintered at 650°C for 5h

Perovskite (pH = 3.5)	a (Å)	b (Å)	c (Å)	V (Å)^3	α=β	γ	Crystal-lite Size [15]
$Sm_{0.6}Sr_{0.4}MnO_3$	5.48	7.68	5.45	229.60	90°	90.35°	19.8
$Sm_{0.8}Sr_{0.2}MnO_3$	5.41	7.45	5.55	227.40	90°	90.35°	51.1
$Sm_{0.2}Sr_{0.8}MnO_3$	5.42	7.36	5.19	223.92	90°	90.35°	42.6

3.2 Electrochemical Characterization

3.2.1 Cyclic Voltammetry (CV)

The cyclic voltammogram of each oxide film electrode on Ni was recorded in the potential 0.0 - 0.7 V at the scan rate of 20 mV sec^{-1} in 1 M KOH at 25°C to know their redox behaviour Fig. 4 (A & B). Each voltammogram was observed to similar in nature. Each voltammogram consists of pair of peaks i.e. anodic (up) and cathodic (down), just prior to the oxygen evolution. The value of redox peaks is almost similar to the redox couple of the Ni [16]. Thus, in the case of oxide film electrode, these peaks were originated due to the redox reaction at Ni-support in contact with electrolyte [14] through cracks, pores, intercrystalline gaps formed in the catalytic film. Also, the oxides prepared at low temperatures have a hydrophilic character and quickly hydrate in aqueous solutions, soaking the entire film thickness. [16]. However, the stability of the film electrode is not affected from this behaviour of the catalyst. From each voltammogram, the values of cyclic voltammetric parameters such as the anodic and cathodic peak potential (E_{Pa} and E_{Pc} respectively), the peak separation potential (ΔE) and the formal redox potential (E°) were calculated for the surface redox reaction and are given in Table 2. From the data obtained it can be clearly observed that on increasing the scan rates the anodic and cathodic peak shifted towards higher current values. Apart from this the ratio of anodic and cathodic peak current was found to be 2. This indicates that redox process is irreversible [17, 18].

Table 2 Values of the cyclic voltammetric parameters on $Sm_{1-x}Sr_xMnO_3$ (0 ≤ x ≤ 0.8) in 1 M KOH at 25°C (scan rate = 20 mVsec^{-1})

Electrode	E_{Pa}/ mV	E_{Pc}/m V	ΔE_p/m V	E° = (E_{Pa}+E_{Pc})/2 (mV)
$SmMnO_3$ (pH = 3.0)	506	358	148	432
$SmMnO_3$ (pH = 3.5)	538	353	185	445
$SmMnO_3$ (pH = 4.0)	500	357	143	428
$SmMnO_3$ (pH = 4.5)	479	359	120	419
$Sm_{0.8}Sr_{0.2}MnO_3$ (pH = 3.5)	517	329	188	423
$Sm_{0.6}Sr_{0.4}MnO_3$ (pH = 3.5)	542	316	226	429
$Sm_{0.2}Sr_{0.8}MnO_3$ (pH = 3.5)	528	317	211	423
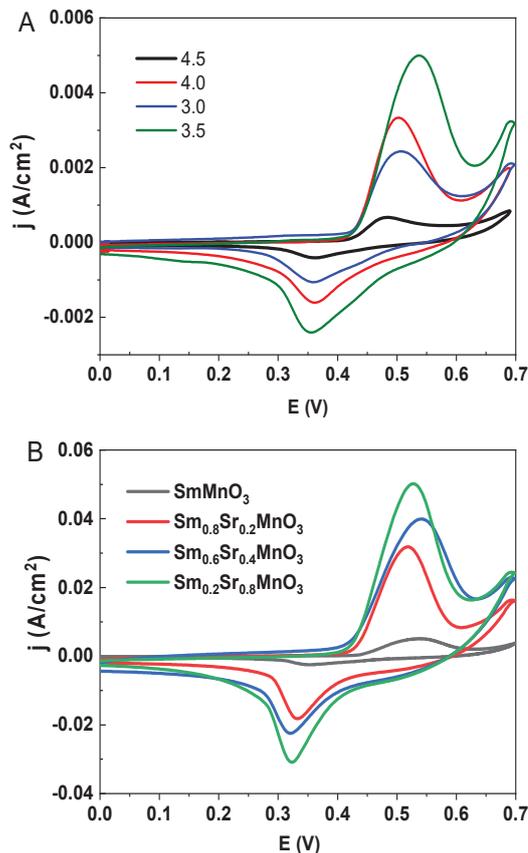
Figure 4 (A): Cyclic voltammograms of $SmMnO_3$ film electrode at different pH on Ni at 20 mV/sec scan rate in 1 M KOH (25°C). **(B)** Cyclic voltammogram of pure and Sr-substituted manganite (pH = 3.5) film electrode on Ni at 20 mV/sec scan rate in 1M KOH (25°C)

The variation of anodic current, cathodic current and voltammetric charge has also been studied with each oxide electrode. The values of │j_P│ vs square root of scan rate was plotted for each oxide electrode and are shown in Fig. 5 (A). From the figure, it is clear that the anodic and cathodic peak current density is linearity varied with square root of scan. The plot of voltammetric charge (q) vs scan rate$^{-1/2}$ was also constructed for each oxide electrode and shown in Fig. 5 (B). The straight line obtained indicates that the surface redox behaviour is diffusion controlled [16].
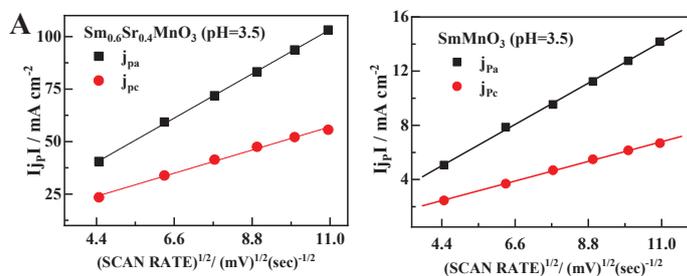
Figure 5 (A): Plot of │j_P│ vs (scan rate)$^{1/2}$ for the oxide film electrodes on Ni in 1M KOH at (25°C)
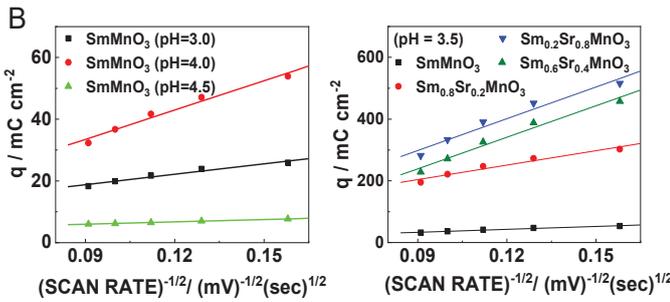
Figure 5 (B): Plot of q vs (scan rate)$^{-1/2}$ for the oxide film electrodes on Ni in 1M KOH at (25°C)

3.2.2 Electrocatalytic activity

The electrocatalytic activity of the oxide film electrode towards OER was determined by recording the Tafel curves (E vs log j) at 0.2 mVsec^{-1} (a slow scan rate) in 1 M KOH at 25°C. The Tafel polarization curves, so obtained, are shown in the Fig. 6 (A). Nature of the polarization curve with each oxide electrode was similar irrespective of the preparation pH and metal ion substitution in the base oxide. The values of Tafel slopes (b), current density (j) at different potentials as well as potential at constant current densities were estimated from the polarization curve and values are given in the Table 3.

The order of OER with respect to OH$^-$ ion concentration was determined by recording Tafel polarization curves at different KOH concentrations (0.25-1.5 M KOH). The ionic strength of the medium was maintained at 1.5 by using an inert electrolyte KNO$_3$. Polarization curve for SmMnO$_3$ (pH = 3.5) & Sm$_{0.6}$Sr$_{0.4}$MnO$_3$ (pH = 3.5) oxide electrodes are shown in Fig. 6 (B) & (C), respectively.

With a constant applied voltage, the value of current density was measured for each oxide catalyst at each concentration with the help of following relation:

$$\eta = a \pm b \log j \qquad (3.1)$$

where η is overpotential and j is current density. 'a' is constant and equals to $\pm b \log j_o$. 'b' is another constant term known as Tafel slope given by relation:

$$b = \frac{d\eta}{d(\log j)_{T,P,\mu}} \qquad (3.2)$$

here T, P and μ are absolute temperature, pressure and ionic strength. The positive and negative sign shows the anodic and cathodic reaction, respectively. Because the second Tafel region was less defined due to increased polarisation at higher potential, the first linear Tafel region of the polarisation curve was typically taken into consideration for this reason. From the data, plot of log j vs. log [OH$^-$] was constructed at a constant potential E = 700 mV and is shown in the Fig. 6 (D). The value of reaction order (p) was estimated measuring the slope of plot of log j vs log [OH$^-$] and given in the Table 3.

3.2.3 Thermodynamic Parameters

On each oxide electrode, the impact of temperature on OER has also been investigated. Anodic polarisation curves in 1 M KOH at various temperatures were acquired for the purpose. The polarization curves, so obtained are shown in Fig. 7 (A) & (B). The reference electrode's temperature was kept constant throughout the experiment.

Table 3: Electrode kinetic parameters for oxygen evolution reaction on Sm$_{1-x}$Sr$_x$MnO$_3$ (0 ≤ x ≤ 0.8) in 1 M KOH at 25°C

Electrode	Tafel slope / mVd^{-1}	E/ mV at j (mA cm^{-2})		j (mA cm^{-2}) at E/mV	
		10	100	700	800
SmMnO$_3$ (pH=3.0)	116	858	1075	0.9	4.2
SmMnO$_3$ (pH=3.5)	107	797	1046	2.4	10.4
SmMnO$_3$ (pH=4.0)	88	924	1151	0.4	2.3
SmMnO$_3$ (pH=4.5)	123	890	1119	0.7	3.2
Sm$_{0.8}$Sr$_{0.2}$MnO$_3$(pH=3.5)	98	678	833	15.6	71.4
Sm$_{0.6}$Sr$_{0.4}$MnO$_3$(pH=3.5)	112	655	782	26.2	126.6
Sm$_{0.2}$Sr$_{0.8}$MnO$_3$(pH=3.5)	108	684	820	15.3	79.4

The slope of the Arrhenius plot, log j versus 1/T [Fig. 7 (C)] determined at a specific potential (E = 700 mV), was used to estimate the standard apparent enthalpy of activation ($\Delta H_{el}^{\circ \#}$). The value of $\Delta H_{el}^{\circ \#}$ varies with potential and found that the value decreases with increasing the potential [Fig. 7 (D)]. The standard enthalpy of activation ($\Delta H^{\circ \#}$) and standard entropy of activation ($\Delta S^{\circ \#}$) were calculated by using following relations (4.1) and (4.2), respectively [19,20];

$$\Delta H_{el}^{\circ \#} = \Delta H^{\circ \#} - \alpha F \eta \qquad (4.1)$$

$$\Delta S^{\circ \#} = 2.3R \left[\log j + \Delta H_{el}^{\circ \#} / 2.3RT - \log (nF\omega C_{OH^-}) \right] \quad (4.2)$$

In equation 4.1, 'α' is the transfer coefficient given by 2.303RT/bF, where R, F and T are the gas constant, Faraday constant and absolute temperature, respectively. 'b' is the Tafel slope (in mV decade^{-1}) determined from the polarization curve recorded at different temperature. η is the overpotential (η= E – E$_{O2/OH^-}$, where E and E$_{O2/OH^-}$ (= 0.303 V vs. Hg/HgO) [21] are the applied potential across the catalyst/1 M KOH interface and the theoretical equilibrium Nernst potential in 1 M KOH at 25 °C, respectively). The terms in equation (4.2) have their usual meaning comprising the frequency term ω (= k$_B$T/h) where, k$_B$ and h are the Boltzmann constant and Planck's constant, respectively. All the calculated thermodynamic parameters are given in the Table 4.1. The most active electrode, Sm$_{0.8}$Sr$_{0.2}$MnO$_3$ (pH = 3.5) was found to have lowest $\Delta H_{el}^{\circ \#}$ value (24.1kJ mol^{-1}). While, it found maximum with SmMnO$_3$ (pH = 4.0).

From the table 4.2, the decrease in standard electrochemical energy of activation ($\Delta H_{el}^{\circ \#}$) can be observed clearly with rise in applied potential. The decrease in $\Delta H_{el}^{\circ \#}$ is also predicted as per equation (4.1) and previous literature [20, 21].
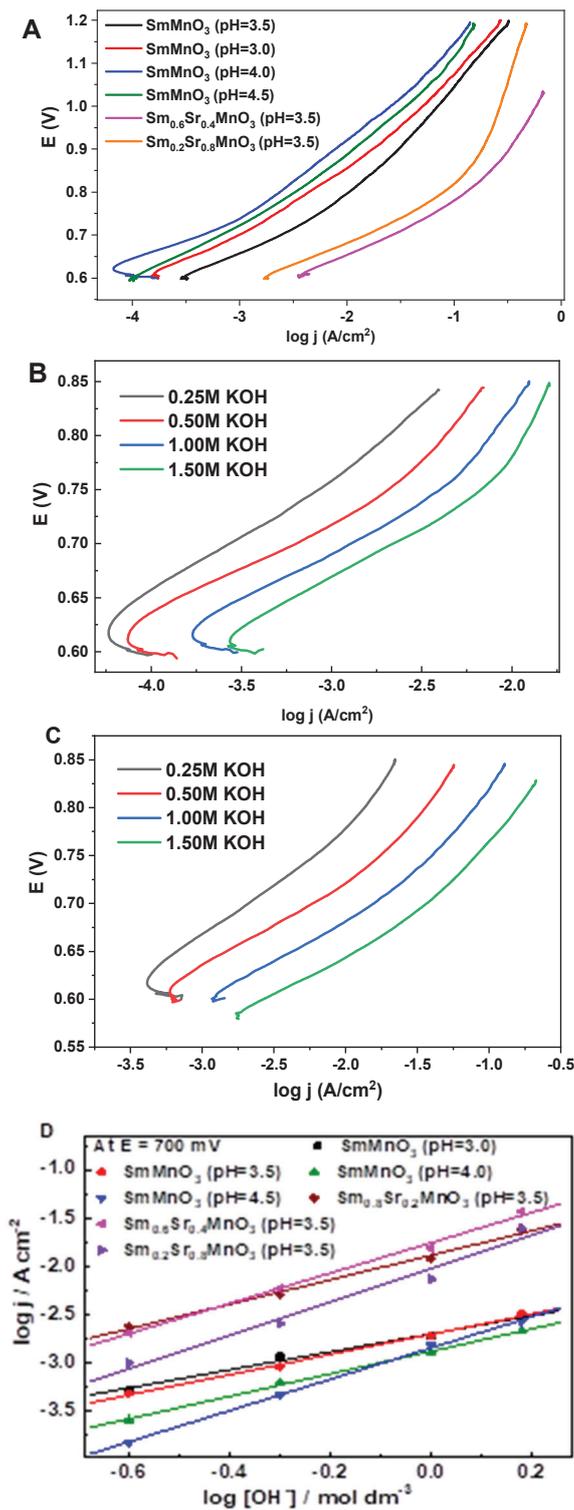
Figure 6(A): Anodic polarization curve for the pure and Sr-substituted samarium manganite film electrodes on Ni in 1M KOH (25°C); scan rate: 0.2mVsec^{-1} **(B)** Anodic polarization curve for the SmMnO$_3$ (pH = 3.5) oxide film electrodes on Ni at different KOH concentrations (μ = 1.5) at 25°C **(C)** Anodic polarization curve for Sm$_{0.6}$Sr$_{0.4}$MnO$_3$ (pH = 3.5) oxide film electrodes on Ni at different KOH concentrations (μ = 1.5) at 25°C **(D)** Plot of log j vs log [OH$^-$] for Ni/Sm$_{1-x}$Sr$_x$MnO$_3$ (0 ≤ x ≤ 0.8) electrodes at 700 mV.

The value of $\Delta S^{\circ \#}$ was found to highly negative which suggests the adsorption phenomena in the oxygen evolution reaction.

Table 4.1 Thermodynamic parameters for O$_2$ evolution on Sm$_{1-x}$Sr$_x$MnO$_3$ (0 ≤ x ≤ 0.8) in 1 M KOH (at E = 700 mV)

Electrode	$\Delta H_{el}^{\circ \neq}$ (kJmol^{-1}) at E = 700 mV	- $\Delta S^{\circ \neq}$ (J deg^{-1} mol^{-1})	α	$\Delta H^{\circ \neq}$ (kJ mol^{-1})
SmMnO$_3$ (pH = 3.0)	48.4	189.9	0.7	76.0
SmMnO$_3$ (pH = 3.5)	38.8	220.7	0.7	66.1
SmMnO$_3$ (pH = 4.0)	65.7	137.8	0.6	89.8
Sm$_{0.8}$Sr$_{0.2}$MnO$_3$ (pH = 3.5)	24.1	239.5	0.9	60.1
Sm$_{0.6}$Sr$_{0.4}$MnO$_3$ (pH = 3.5)	36.4	196.3	0.9	68.9
Sm$_{0.2}$Sr$_{0.8}$MnO$_3$ (pH = 3.5)	44.0	182.0	0.7	71.9

Table 4.2: Thermodynamic parameters for O$_2$ evolution on Sm$_{0.6}$Sr$_{0.4}$MnO$_3$ in 1 M KOH at different potentials (α=0.86)

Potential E (mV)	$\Delta H_{el}^{\circ \neq}$ (kJ mol^{-1})	- $\Delta S^{\circ \neq}$ (J deg^{-1} mol^{-1})	$\Delta H^{\circ \neq}$ (kJ mol^{-1})
625	70.3	102.5	96.9
650	57.4	138.0	86.2
675	38.3	194.8	69.2
700	31.9	210.6	64.9
725	28.7	217.7	63.7

4. CONCLUSION

The study has exposed the synthesis of Samarium substituted strontium manganites (Sm$_{1-x}$Sr$_x$MnO$_3$ (0 ≤ x ≤ 0.8), a perovskite oxide by sol-gel route using malic acid and tested for its electrochemical behaviour towards oxygen evolution reaction. The cyclic voltammetry and the Tafel experiments performed for the same reveals the effect of substitution of strontium by samarium in the lattice of the strontium manganites. The optimum improvement in the Tafel slope value has been seen in the highly substituted strontium manganite i.e., Sm$_{0.8}$Sr$_{0.2}$MnO$_3$ (pH = 3.5) while the highest current density value (126.6 mA cm^{-2}) at 800 mV was observed in the case of Sm$_{0.6}$Sr$_{0.4}$MnO$_3$. Apart from this the synthesised perovskite oxide are also analysed for their thermodynamic and kinetic parameters for oxygen evolution reaction.
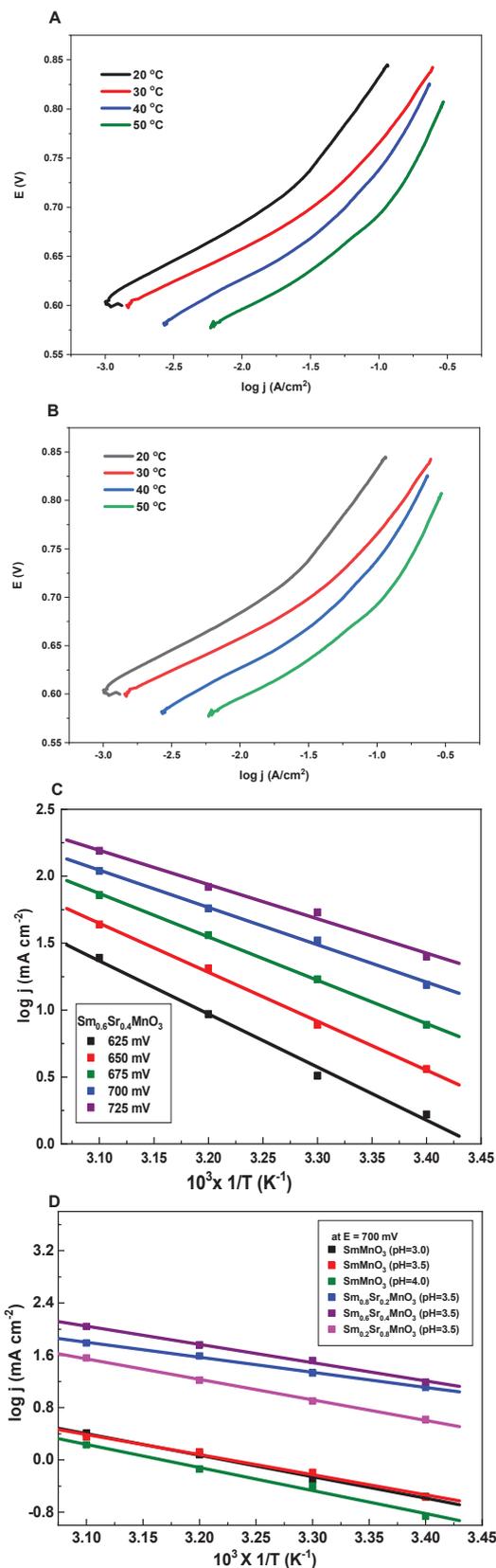
Figure 7 (A): Anodic polarization curve of the $SmMnO_3$ (pH=3.5) film electrode on Ni at different temperature. **(B):** Anodic polarization curve of the $Sm_{0.6}Sr_{0.4}MnO_3$ (pH = 3.5) film electrode on Ni at different temperature. **(C):** The Arrhenius plot of $Sm_{1-x}Sr_xMnO_3$ ($0 \leq x \leq 0.8$) in 1 M KOH at a constant applied potential (E = 700 mV) **(D):** The Arrhenius plot of $Sm_{0.6}Sr_{0.4}MnO_3$ in 1 M KOH at different applied potentials.

REFERENCES

[1]. O'Sullivan, E.; Calvo, E., In Electrode Kinetic Reaction. ed. R. G. Compton, Elsevier, Amsterdam 1987, 274.

[2]. Furlong, D.; Yates, D.; Healy, T.; Trasatti, S., Electrodes of conductive metallic oxides, Part B. Elsevier, Amsterdam: 1981.

[3]. Wendt, H.; Imarisio, G., Nine years of research and development on advanced water electrolysis. A review of the research programme of the Commission of the European Communities. J. Appl. Electrochem. 1988, 18, 1-14. https://doi.org/10.1007/BF01016198

[4]. Matsumoto, Y.; Yoneyama, H.; Tamura, H., The mechanism of oxygen reduction at a LaNiO3 electrode. Bull. Chem. Soc. Jpn., 1978, 51 (7), 1927-1930. https://doi.org/10.1246/bcsj.51.1927

[5]. Ladavos, A.; Pomonis, P., Comparative study of the solid-state and catalytic properties of La 2–x Sr x NiO 4λ perovskites (x= 0.00–1.50) prepared by the nitrate and citrate methods. J. Chem. Soc., Faraday Trans., 1991, 87 (19), 3291-3297. https://doi.org/10.1039/FT9918703291

[6]. Suntivich, J.; May, K. J.; Gasteiger, H. A.; Goodenough, J. B.; Shao-Horn, Y., A perovskite oxide optimized for oxygen evolution catalysis from molecular orbital principles. Science 2011, 334 (6061), 1383-1385. https://doi.org/10.1126/science.1212858

[7]. Tiwari, S.; Chartier, P.; Singh, R., Preparation of Perovskite-Type Oxides of Cobalt by the Malic Acid Aided Process and Their Electrocatalytic Surface Properties in Relation to Oxygen Evolution. J. Electrochem. Soc, 1995, 142 (1), 148. https://doi.org/10.1149/1.2043854

[8]. Bockris, J. O. M.; Otagawa, T. J. J. o. T. E. S., The electrocatalysis of oxygen evolution on perovskites. J. Electrochem. Soc., 1984, 131 (2), 290. https://doi.org/10.1149/1.2115565

[9]. Balej, J., Electrocatalysts for oxygen evolution in advanced water electrolysis. Int. J. Hydrog. Energy, 1985, 10 (2), 89-99. https://doi.org/10.1016/0360-3199(85)90041-2

[10]. Kobussen, A.; Van Buren, F.; Van den Belt, T.; Van Wees, H., Oxygen evolution on LaCoO3-type electrodes. J. Electroanal. Chem., 1979, 96 (1), 123-125.https://doi.org/10.1016/S0022-0728(79)80309-5

[11]. Matsumoto, Y.; Manabe, H.; Sato, E. J. J. o. T. E. S., Oxygen evolution on La1− xSrxCoO3 electrodes in alkaline solutions. J. Electrochem. Soc. 1980, 127 (4), 811. 10.1149/1.2129762

[12]. Wendt, H.; Plzak, V., Electrocatalytic and thermal activation of anodic oxygen-and cathodic hydrogen-evolution in alkaline water electrolysis. Electrochim. Acta 1983, 28 (1), 27-34. https://doi.org/10.1016/0013-4686(83)85083-X

[13]. Teraoka, Y.; Kakebayashi, H.; Moriguchi, I.; Kagawa, S., Hydroxy acid-aided synthesis of perovskite-type oxides of cobalt and manganese. Chem. Lett., 1991, 20 (4), 673-676. https://doi.org/10.1246/CL.1991.673

[14]. Singh, R. N.; Tiwari, S. K.; Singh, S. P.; Singh, N. K.; Poillerat, G.; Chartier, P., Synthesis of (La, Sr) CoO3 perovskite films via a sol–gel route and their physicochemical and electrochemical surface characterization for anode application in alkaline water electrolysis. J. Chem. Soc., Faraday Trans., 1996, 92

(14), 2593-2597.
https://doi.org/10.1039/FT9969202593

[15]. Fradette, N.; Marsan, B., Surface Studies of CuxCo3−xO4 Electrodes for the Electrocatalysis of Oxygen Evolution. J. Electrochem. Soc., 1998, 145 (7), 2320. 10.1149/1.1838637

[16]. Singh, N.; Tiwari, S.; Anitha, K.; Singh, R., Electrocatalytic properties of spinel-type MnxFe3−xO4synthesized below 100°C for oxygen evolution in KOH solutions. J. Chem. Soc., Faraday Trans., 1996, 92 (13), 2397-2400.
https://doi.org/10.1039/FT9969202397

[17]. Wu, W.; Guo, S.; Zhang, J., Electrochemical behaviors of Cr (III) in molten LiF-NaF-KF eutectic. Int. J. Electrochem. Sci., 2018, 13, 225-234.
http://dx.doi.org/10.20964/2018.01.21

[18]. Massot, L.; Chamelot, P.; Cassayre, L.; Taxil, P., Electrochemical study of the Eu (III)/Eu (II) system in molten fluoride media. Electrochim. Acta, 2009, 54 (26), 6361-6366.
https://doi.org/10.1016/j.electacta.2009.06.016

[19]. Singh, N. K.; Sharma, P.; Kumar, I.; Chaddha, A. S., Oxygen evolution electrocatalytic properties of perovskite-type La1-xSrxCoO3 (0≤ x≤ 0.8) oxides obtained by polyvinylpyrroli-done sol-gel route. Int. J. Electrochem. Sci 2019, 14, 11379-11390. 10.20964/2019.12.70

[20]. E. Gileadi, "Electrode Kinetics", VCH Publishers Inc., New York, 1993, p.151.

[21]. R. Singh, J. Pandey, N. Singh, B. Lal, P. Chartier, J.-F. Koenig, Sol-gel derived spinel $M_xCo_{3-x}O_4$ (M= Ni, Cu; 0≤ x≤ 1) films and oxygen evolution, *Electrochim. Acta,* 45 (2000) 1911-1919. http://dx.doi.org/10.1016/S0013-4686(99)00413-2

[22]. Singh, N.; Yadav, R.; Yadav, M., Electrocatalytic Properties of Egg-white Sol-gel Derived $Mn_xFe_{3-x}O_4$ (0≤ x≤ 1.5) for Alkaline Water Electrolysis. *J. New Mater. Electrochem. Syst.,* 19(2016) 209-215. http://dx.doi.org/10.14447/jnmes.v19i4.281

[23]. Singh, N.; Singh, J.; Singh, R., Sol–gel-derived spinel Co_3O_4 films and oxygen evolution: Part II. Optimization of preparation conditions and influence of the nature of the metal salt precursor. *Int. J. Hydrogen Energy,* **2002,** *27* (9), 895-903. https://doi.org/10.1016/S0360-3199(01)00193-8